Devil's Staircase in the Magnetoresistance of a Periodic Array of Scatterers

Jan Wiersig and Kang-Hun Ahn

Max-Planck-Institut für Physik komplexer Systeme, Nöthnitzer Strasse 38, 01187 Dresden, Germany

The nonlinear response to an external electric field is studied for classical noninteracting charged particles under the influence of a uniform magnetic field, a periodic potential, and an effective friction force. We find numerical and analytical evidence that the ratio of transverse to longitudinal resistance forms a Devil's staircase. The staircase is attributed to the dynamical phenomenon of mode-locking.

The electron transport in two-dimensional periodic arrays of scatterers has been actively studied for the last decade. One of the most interesting features is the plateaulike behavior in Hall resistance as well as peaks in magnetoresistance [1,2] at low magnetic fields below the quantum Hall regime. The peak structure in magnetoresistance has been attributed to the electron cyclotron orbits which enclose an *integer* number of scatterers [2,3]. The cyclotron motion is important when the electron mean free path l (l is measured in the absence of periodic scatterers) is greater than the period a of the regular scatterers.

In this Letter, we present a theory for electron transport in the deeply *diffusive* regime $l \ll a$ where cyclotron motion is not relevant. We predict a new and interesting effect where the structure in the magnetoresistance is associated with *fractional* numbers. We will show that the relative ratio between the transversal and longitudinal magnetoresistance forms a *Devil's staircase*. These fractal staircases originate from a dynamical phenomenon known as *mode-locking* which appears naturally in the context of *circle maps* [4]. Our prediction is based on the finding that the dynamics in a two-dimensional periodic array of scatterers with intrinsic momentum relaxation effectively reduces to a circle map.

Let us consider first a particle of mass m, charge q in crossed electric ($\boldsymbol{E} = E\hat{\boldsymbol{x}}$), and magnetic fields ($\boldsymbol{B} = -B\hat{\boldsymbol{z}}$) with intrinsic momentum relaxation. The resulting drift motion $\boldsymbol{x}(t) = [x(t), y(t)]$ can be described by adding a frictional force, proportional to the drift velocity $\boldsymbol{v}$, to the equations of motion yielding

$$
\begin{aligned}
\dot{x} = v_x, &\qquad m\dot{v}_x = -qBv_y + qE - mv_x/\tau, \\
\dot{y} = v_y, &\qquad m\dot{v}_y = qBv_x - mv_y/\tau,
\end{aligned}
\tag{1}
$$

with τ being the momentum relaxation time. Cyclotron motion exists only for a transient time; each trajectory finally converges to a straight line with the time-averaged velocity $\langle\boldsymbol{v}\rangle = (m/\tau, qB)qE/(q^2B^2 + m^2/\tau^2)$. With the charge density n and the current density $\boldsymbol{J} = qn\langle\boldsymbol{v}\rangle$, it is easy to calculate the resistivities defined by $\boldsymbol{E} = \hat{\rho}\boldsymbol{J}$ and Onsager's relations $\rho_{xx} = \rho_{yy}$ and $\rho_{yx} = -\rho_{xy}$: the diagonal resistivity $\rho_{xx} = m/q^2 n\tau$ is constant, whereas the off-diagonal resistivity $\rho_{xy} = B/qn$ depends linearly on the magnetic field—no plateaus are present.

We now add a periodic potential $V = V_0 F(\boldsymbol{x})$ with $|F|$ of order one to the equations of motion (1), assuming that the periodicity of the potential, a, is much larger than the length scale related to the intrinsic momentum relaxation. When we scale the coordinates $\boldsymbol{x}$ with a and the time t with τ, we get the same equations of motion for a given set of three dimensionless parameters: $\tilde{B} = q\tau B/m$, $\tilde{E} = q\tau^2 E/(ma)$, and $\tilde{V}_0 = V_0/(qEa)$. We use the rescaled magnetic field $\tilde{B}$ as a variable parameter and fix the rescaled electric field and potential strength to $\tilde{E} = 0.07$ and $\tilde{V}_0 = 0.12$ if not otherwise stated. Though we could choose various sets of parameters (τ, a, E, etc.) for the chosen values of $\tilde{E}$ and $\tilde{V}_0$, for definiteness we will take $\tau = 7.6 \times 10^{-14}$ s, $E = -2.3 \times 10^4$ V/cm, and $a = 0.5$ μm, and fix these for the rest of the paper. The particle is an electron in GaAs sample with $q = -e$ and $m = 0.067m_e$. By taking a typical value of Fermi velocity $v_f \approx 3 \times 10^7$ cm/s, the mean free path of our system is $l = v_f\tau \approx 0.02$ μm $\ll a$.

First, we show how the particle's motion is related to a one-dimensional circle map through analytical considerations for sufficiently small potential strength. Note that our numerics do not rely on this requirement. Because of the periodicity of the potential it is sufficient to consider the unit cell of the potential with periodic boundary conditions; i.e., we can compactify the (x, y) plane to a two-dimensional torus. A typical asymptotic solution for zero potential strength as discussed above appears here as a quasiperiodic trajectory filling densely a two-dimensional invariant torus $\boldsymbol{v} = $ const in four-dimensional phase space. Trajectories starting away from the torus are attracted towards it and asymptotically converge onto it. For finite potential strength the torus is smoothly deformed or collapsed into lower-dimensional objects or broadened to a higher-dimensional object (loosely speaking, a torus with finite but very small thickness). The latter possibility can be ignored to a very good approximation as we will see later. A point on the torus (and on the lower-dimensional objects) is uniquely labeled by unit-cell coordinates ($x_1 \bmod 1, x_2 \bmod 1$) defined by $\boldsymbol{x} = x_1\boldsymbol{a}_1 + x_2\boldsymbol{a}_2$, with $\boldsymbol{a}_1 = (a_{11}, a_{12})$, $\boldsymbol{a}_2 = (a_{21}, a_{22})$ being the lattice vectors of the unit cell. The long-time behavior is therefore completely described by two-dimensional dynamics

$[x_1(t), x_2(t)]$. As usual, such dynamics can be conveniently investigated by introducing *Poincaré surfaces of section* defined by $x_1(t_n) \bmod 1 = 0$, where n is an integer and modulo 1 restricts the variable to the interval $[0, 1)$.

The discrete evolution of $x_{2,n} \equiv x_2(t_n)$ is then governed by a one-dimensional map $x_{2,n+1} = f(x_{2,n})$ where f is a smooth and monotonic function. Because of the periodicity of the potential the condition $f(x_2) \bmod 1 = f(x_2 \bmod 1)$ holds. Such a map is called an *invertible circle map*. Its *rotation number*,

$$\rho \equiv \lim_{n \to \infty} \frac{x_{2,n} - x_{2,0}}{n}, \qquad (2)$$

is well defined and independent of the initial condition $x_{2,0}$ [4]. A rational value of $\rho = p/q$ (p and q are integers without common divisor) indicates periodic motion, whereas an irrational value indicates quasiperiodic motion; chaotic motion is not possible.

We now derive a simplified circle map valid in the limit $\tilde{V}_0 \ll 1$. If $\tilde{V}_0 = 0$ then the asymptotic dynamics obeys $\dot{v}_x = \dot{v}_y = 0$, leading to $f(x_2) = x_2 + \rho_0$ with the constant $\rho_0(\tilde{B})$; here we have simply $\rho = \rho_0$, so ρ_0 can be regarded as the unperturbed rotation number. The asymptotic dynamics for nonzero but sufficiently small $\tilde{V}_0$ is overdamped, i.e., $|\dot{v}_x| \ll |v_x|/\tau$ and $|\dot{v}_y| \ll |v_y|/\tau$. As in the potential-free case, the number of differential equations reduces to two, enabling us to determine f up to first order in $\tilde{V}_0$

$$f(x_{2,n}; \rho_0, \tilde{E}, \tilde{V}_0) \approx x_{2,n} + \rho_0 + \tilde{V}_0 g(x_{2,n}; \rho_0) \qquad (3)$$

with

$$g = \frac{\rho_0^2(a_{22}^2 + a_{21}^2) + 2\rho_0(a_{11}a_{21} + a_{12}a_{22}) + a_{12}^2 + a_{11}^2}{(a_{11}a_{22} - a_{21}a_{12})^2} \int_0^1 \left(a_{21} \frac{\partial F}{\partial x_1} - a_{11} \frac{\partial F}{\partial x_2} \right)\Bigg|_{x_2 = \rho_0 x_1 + x_{2,n}} dx_1, \qquad (4)$$

where g is a nontrivial periodic function of $x_{2,n}$. Note that f is independent of the parameter $\tilde{E}$ in the present approximation. Using Stoke's theorem it can be shown that $\int_0^1 g \, dx_2 = 0$. For circle maps of the form given in Eq. (3) with the above-mentioned properties of g it is proven that for each $\tilde{V}_0$ there exists a Devil's staircase, a monotonically increasing function $\rho = \rho(\rho_0)$ with plateaus at each rational value of ρ. The width of the plateaus, $\Delta \rho_0$, is proportional to $\tilde{V}_0$ [5]. Similarly, the widths of the plateaus, $\Delta \tilde{B}$, of the function $\rho = \rho(\tilde{B})$, are proportional to $\tilde{V}_0$ since $\Delta \tilde{B} \approx (d\tilde{B}/d\rho_0)\Delta \rho_0$.

The rotation number ρ is directly related to the continuous-time dynamics. This can be seen by rewriting Eq. (2) with $\boldsymbol{v} = v_1 \boldsymbol{a}_1 + v_2 \boldsymbol{a}_2$ as

$$\rho = \frac{\langle v_2 \rangle}{\langle v_1 \rangle} = \frac{-a_{12} + a_{11}\langle v_y \rangle / \langle v_x \rangle}{a_{22} - a_{21}\langle v_y \rangle / \langle v_x \rangle} = \frac{-a_{12} + a_{11}\sigma_{xy}/\sigma_{xx}}{a_{22} - a_{21}\sigma_{xy}/\sigma_{xx}}. \qquad (5)$$

Hence, ρ is given by the ratio of the conductivities. In the case that the periodic potential is invariant under π/m rotations, $m = 2, 3, \ldots$, Onsager's relations show that ρ can also be expressed by the ratio ρ_{xy}/ρ_{xx}.

We now present numerical evidence showing that for finite $\tilde{V}_0 \lesssim 0.4$ the continuous-time dynamics is indeed given by a one-dimensional circle map and that the magnetoresistance shows a fractal structure. As an example of the periodic scatterers, we take a potential with hexagonal symmetry shown in Fig. 1a,

$$V(x, y) = V_0 \Bigg\{ \left[\cos\left(\frac{\pi}{3} (\sqrt{3}x - y) \right) \cos\left(\frac{2\pi}{3} y \right) \right]^\beta + \left[\cos\left(\frac{\pi}{3} (\sqrt{3}x + y) \right) \cos\left(\frac{\pi}{3} (\sqrt{3}x - y) \right) \right]^\beta$$

$$+ \left[\cos\left(\frac{2\pi}{3} y \right) \cos\left(\frac{\pi}{3} (\sqrt{3}x + y) \right) \right]^\beta \Bigg\}, \qquad (6)$$

with $\beta = 8$. The lattice vectors are $\boldsymbol{a}_1 = (\sqrt{3}, 0)$ and $\boldsymbol{a}_2 = (-\sqrt{3}/2, -3/2)$. We have used the Runge-Kutta method [6] with 10^6 time steps of variable size to integrate the equations of motion. We found that all initial conditions, for fixed parameters, lead to the same mean velocity $\langle \boldsymbol{v} \rangle$. So only one single orbit is needed to calculate the current density and the resistivities without employing the Kubo formula [7]. This already indicates the collapse to an invertible circle map. To show the reduction to the map explicitly, we calculate a sequence of points $(x_{2,n} \bmod 1, x_{2,n+1} \bmod 1)$ by solving the complete set of differential equations for different initial velocities from one Poincaré section to the next. Figures 2a and 2b show that these points indeed lie very close to a line, so $x_{2,n+1}$ is to excellent approximation a function of $x_{2,n}$ independent of the initial velocity. We have computed $(x_{2,n+1} - x_{2,n} - \rho_0)/\tilde{V}_0$ for different parameters $\tilde{V}_0$ and

$\tilde{E}$. It can be seen from Fig. 2c that this quantity is roughly independent of $\tilde{V}_0$, even though small deviations indicate weak nonlinear behavior in $\tilde{V}_0$. Figure 2d shows that $(x_{2,n+1} - x_{2,n} - \rho_0)/\tilde{V}_0$ does not change when $\tilde{E}$ is varied over 2 orders of magnitude. Figures 2a–2d therefore confirm the reduction to the circle map and its parameter dependence as predicted in Eq. (3).

Figure 3 is our main result. It shows the Devil's staircase ρ vs ρ_0. Both quantities are computed from the resistivities via the relations $\rho = 2/(1 + \sqrt{3}\,\rho_{xx}/\rho_{xy})$ and $\rho_0 = 2/(1 - \sqrt{3}/\tilde{B})$ from Eq. (5) with the lattice vectors of the rotational symmetric potential (6). Note the exactness of the plateaus. Let us discuss some features of the Devil's staircase in relation to the continuous and discrete-time dynamics. Figures 1b and 1c show two orbits moving in slightly different magnetic fields. Both
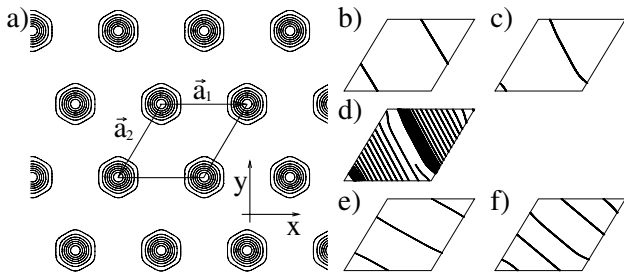
FIG. 1. (a) Contour plot of the potential in Eq. (6) with $\beta = 8$. (b) Orbit with $B = 8.7$ T and $\rho = 1$ in the unit cell. (c) $B = 9.77$ T and $\rho = 1$. (d) 9.8 T and $\rho = 1.014\,07\ldots$ (e) 2.9 T and $\rho = 1/2$. (f) 4.4 T and $\rho = 2/3$.

have synchronized velocities $\langle v_1 \rangle = \langle v_2 \rangle$, i.e., $\rho = 1$. Each orbit with $\rho = 1$ is a stable fixed point $x_2^* = f(x_2^*)$ in the corresponding map (filled circles in Figs. 2a and 2b; empty circles mark unstable fixed points). This synchronization phenomenon, usually called *mode-locking* in nonlinear dynamics, is therefore due to the robustness of fixed points under variation of a parameter, here $\rho_0(B)$. Orbits with $\rho \neq 1$ are in a different *mode*; in particular, orbits with irrational rotation number are not periodic. In Fig. 1d we see an orbit with irrational ρ close to one. It stays for a long time near a periodic orbit with $\rho = 1$ but from time to time it escapes, thereby filling the entire unit cell densely. This phenomenon is often called *intermittency* in chaotic dynamics [8]. In terms of the circle map, the transition from $\rho = 1$ to irrational ρ is a saddle-node bifurcation: as B is varied, stable and unstable fixed points come closer and closer as illustrated in Figs. 2a and 2b, and finally destroy each other, yielding

FIG. 3. Rotation number ρ vs ρ_0. Arrows assign the rational value of the rotation number $\rho = p/q$ to each plateau. The inset highlights the fractal structure of the Devil's staircase.

quasiperiodic motion. Varying B further can lead again to periodic motion. Figures 1e and 1f give two examples with $\rho = 1/2$ and $\rho = 2/3$. The corresponding map has a stable fixed point of higher period, e.g., for $\rho = 1/2$ the fixed point condition is $x_2^* = f[f(x_2^*)]$.

We also observe a Devil's staircaselike function $\rho_{xy}(B)$ in Fig. 4, which reminds one of the quantum Hall effects [9,10], but here the "plateaus" are not perfectly flat. One may note also that the way ρ_{xx} varies for a number of ρ_{xy} plateaus has similarities to the quantum Hall effects: going from the center of a ρ_{xy} plateau towards its border, ρ_{xx} increases and reaches its maximum exactly when the plateau ends. This can be explained qualitatively. First, note that an orbit from the center of the $\rho = 1$ plateau (Fig. 1b) avoids the potential's steep maxima at the corners of the unit cell. Hence, the diagonal resistivity roughly equals the
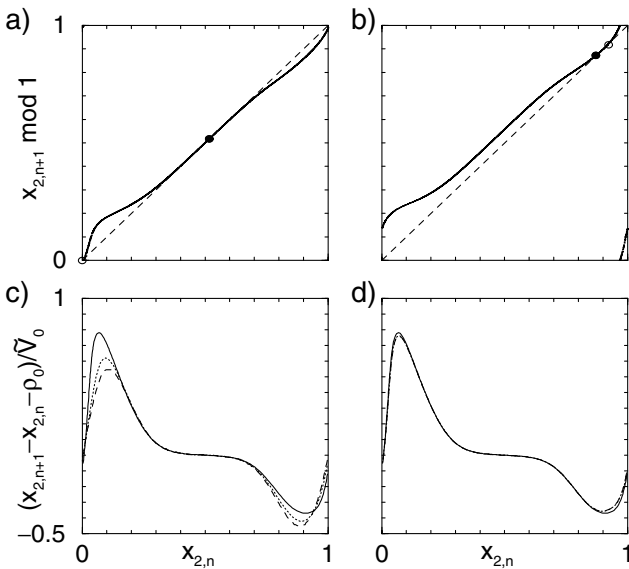

FIG. 2. (a) $x_{2,n+1} \bmod 1$ vs $x_{2,n}$ for $B = 8.7$ T. (b) 9.77 T. (c) $(x_{2,n+1} - x_{2,n} - \rho_0)/\tilde{V}_0$ vs $x_{2,n}$ for $B = 8.7$ T, $\tilde{V}_0 = 0.12$, and $\tilde{E} = 0.07$ (solid line); $\tilde{V}_0 = 0.06$ (dotted line); $\tilde{V}_0 = 0.03$ (dashed line). (d) $\tilde{V}_0 = 0.12$, and $\tilde{E} = 0.07$ (solid line); $\tilde{E} = 0.007$ (dotted line); $\tilde{E} = 0.0007$ (dashed line).
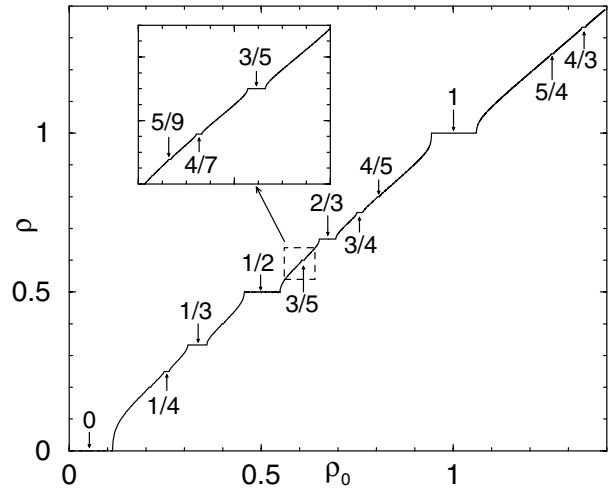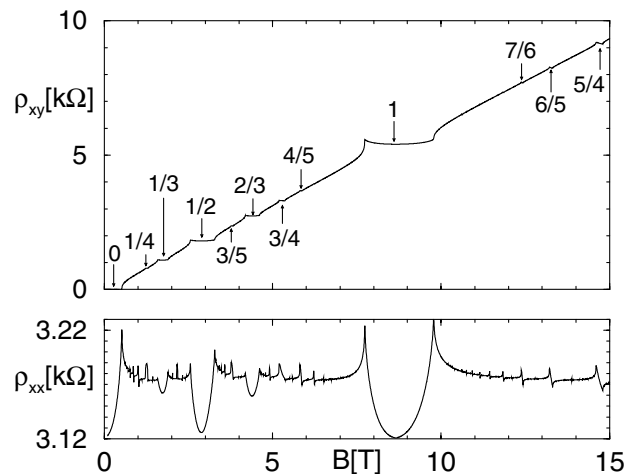

FIG. 4. Off-diagonal resistivity ρ_{xy} and diagonal resistivity ρ_{xx} vs magnetic field B. Arrows assign the rational value of the rotation number $\rho = p/q$ to each plateau. We here have used $n = 10^{12}$ cm^{-2}.
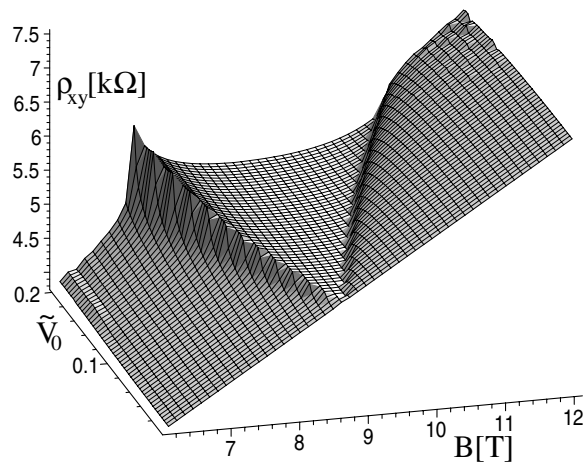
FIG. 5. Dependence of the $\rho = 1$ plateau on $\tilde{V}_0$; cf. Fig. 4.

potential-free value $\rho_{xx} = m/q^2 n\tau \approx 3.12$ kΩ. We infer from Figs. 1b and 1c that the closer B is to the border of the plateau the closer is the orbit to the potential's maxima. This effectively slows down the orbit, which explains the increase of ρ_{xx} (and ρ_{xy}). Leaving the plateau reduces ρ_{xx} continuously because of the intermittency effect, which becomes less pronounced with increasing $|\rho - 1|$.

The example in Fig. 5 confirms that the widths of the plateaus, ΔB, is roughly proportional to $\tilde{V}_0$ as predicted from the analysis of the simplified circle map in Eq. (3). By noting that $\tilde{V}_0$ denotes the dimensionless potential strength we see an interesting analogy with the quantum Hall effect where the size of plateaus is sensitive to the disorder strength of the systems [11]. Here we have the advantage of the use of the simplified circle map to analyze the plateau size, although the overall structure of the hierarchy of the plateaus is also too complicated to be dealt with in an analytic fashion.

Since the particle can be trapped in the very flat local minima of the potential (6), a finite dc electric field is necessary to overcome the potential trap as in the experiment in Ref. [12]. The threshold [13] value E_T of the electric field for the finite electrical current might be crudely estimated by $E_T \sim V_0/(qa)$, which is in agreement with our calculations (not shown). However, in reality the threshold electric field will be much smaller in the presence of the degenerate electron gas because the weak local trap potential will be screened [14]. While we have chosen in our numerical calculation a large electric field (2.3×10^4 V/cm) and a low mobility of the sample ($\mu = e\tau/m \approx 2000$ cm^2/V s), the Devil's staircase may be observed in a broad range of parameters. We also note that the specific form of the potential (6) is not relevant. However, the steepness of the potential influences the shape of the ρ_{xy} plateaus. Large steepness (large β) results in wide and curved ρ_{xy} plateaus. It should be mentioned also that the Devil's staircase will not be seen in the

conventional Hall bar where the electrical current is fixed along the bar and the induced Hall voltage is measured. To measure the electrical current in two-dimensional samples for fixed applied voltages, one needs to use metallic leads which span the entire length of two opposite edges of the sample [14].

In summary, we have calculated the magnetoresistance of a lateral surface superlattice with strong momentum relaxation where the cyclotron motion is not involved. Our calculations show a fractal plateau structure in the magnetoresistance which stems from purely classical nonlinear dynamics. We have explained our calculational results in terms of the theory of circle maps where the Devil's staircase is already well understood.

[1] K. Ensslin and P. M. Petroff, Phys. Rev. B **41**, 12 307 (1990).
[2] D. Weiss, M. L. Roukes, A. Menschig, P. Grambow, K. von Klitzing, and G. Weimann, Phys. Rev. Lett. **66**, 2790 (1991); for more works on lateral surface superlattices see, e.g., D. Weiss, in *Festkörperprobleme, Advances in Solid State Physics* (Vieweg, Braunschweig, 1991), Vol. 31; C. W. J. Beenakker and H. van Houten, in *Solid State Physics* (Academic, San Diego, 1991), Vol. 44.
[3] R. Fleischmann, T. Geisel, and R. Ketzmerick, Phys. Rev. Lett. **68**, 1367 (1992).
[4] See, e.g., D. Arrowsmith and C. Place, *An Introduction to Dynamical Systems* (Cambridge University Press, Cambridge, 1990).
[5] G. R. Hall, SIAM J. Math. Anal. **15**, 1075 (1984).
[6] W. H. Press, B. P. Flannery, S. A. Teukolsky, and W. T. Vetterling, *Numerical Recipes in C* (Cambridge University Press, Cambridge, 1988).
[7] R. Kubo, J. Phys. Soc. Jpn. **12**, 570 (1957).
[8] See, e.g., E. Ott, *Chaos in Dynamical Systems* (Cambridge University Press, Cambridge, 1993).
[9] K. von Klitzing, G. Dorda, and M. Pepper, Phys. Rev. Lett. **45**, 494 (1980).
[10] D. C. Tsui, H. L. Stormer, and A. C. Gossard, Phys. Rev. Lett. **48**, 1559 (1982).
[11] See, e.g., M. Janssen, O. Viehweger, U. Fastenrath, and J. Hajdu, *Introduction to the Theory of the Integer Quantum Hall Effect* (VCH Verlagsgesellschaft mbH, Weinheim, 1994).
[12] G. M. Gusev, Z. D. Kvon, A. G. Pogosov, and M. M. Voronin, JETP Lett. **65**, 248 (1997).
[13] The threshold behavior is also seen in the charge-density-wave transport; see for a review G. Grüner, *Density Waves in Solids* (Addison-Wesley, Reading, MA, 1994). Devil's staircases appear in these systems if both ac and dc electric fields are applied; see P. Bak, T. Bohr, and M. H. Jensen, Phys. Scr. **T9**, 50 (1985).
[14] K. v. Klitzing (private communication).